www.czasopisma.pan.pl PAN POLSKA AKADEMIA NAUK www.journals.pan.pl

ARCHIVES OF ACOUSTICS
36, 3, 575–601 (2011)

DOI: 10.2478/v10168-011-0041-9

3D Multi-Domain MFS Analysis of Sound Pressure Level Reduction Between Connected Enclosures

Luís GODINHO, Fernando G. BRANCO, Paulo AMADO MENDES

University of Coimbra
CICC, Department of Civil Engineering
Pólo 2 – FCTUC
Rua Luís Reis Santos, 3030-788 Coimbra, Portugal
e-mail: lgodinho@dec.uc.pt

(*received November 3, 2010; accepted February 28, 2011*)

In this paper, the authors study the 3D propagation of sound waves between two closed spaces. The separation element between the two rooms is considered to include either a small opening or a homogeneous lightweight panel, coupling the two spaces. A numerical study of this configuration is performed, trying to understand the influence of the position and geometry of this opening in the sound pressure level reduction curve at low and midfrequencies. Additionally, the coupling effect between the two acoustic spaces is analyzed, in order to better understand its importance when determining the sound pressure level reduction. Different boundary conditions are ascribed to the walls of these rooms, simulating both the completely reflecting and partially absorbing surfaces.

The numerical modelling was performed using a multi-domain formulation of the Method of Fundamental Solutions (MFS). The system is composed of two coupled rooms, limited by rigid or by absorbing walls, and separated by a thin wall (tending to null thickness) with a small opening. An experimental validation of the proposed model is presented, comparing its results with those found experimentally for a reduced-scale model. It is important to note that, for such a configuration, a traditional single-domain approach using methods like the MFS or the BEM would lead to undetermined equation systems, and thus the proposed model makes use of a domain decomposition technique.

Keywords: Method of Fundamental Solutions, domain decomposition, closed spaces, sound pressure level reduction.

1. Introduction

The transmission of sound between two rooms separated by a partition wall is a complex dynamic problem, involving many variables. Among these, the physical and elastic properties of the partition element and the incident sound frequency

are usually considered as dominant. It is known that there is a strong relation between sound insulation and the element mass, with the inertial forces playing a dominant role. As for the incident frequency, it is known that the vibration power of a partition diminishes as the sound frequency increases which, together with a higher energy dissipation capability, leads to an increase in sound insulation for higher excitation frequencies. However, other dynamic phenomena, such as the coincidence effect or the structural modes of the element, can originate insulation dips, and can even hinder the development of the insulation increase with the frequency in some cases.

This topic has interested researchers over the years, and many prediction models have been proposed to estimate the sound insulation provided by a wall. One of the best known prediction models is the mass law (see, for example, Beranek and Ver, 1992), which has been extensively applied to study the sound insulation provided by many types of partition walls. However, the limitations of this model have stimulated the development of more complex models, such as those proposed by Sharp (1978) or by Tadeu and António (2002).

The above mentioned models are usually applicable to homogeneous partitions and allow taking into account a large number of aspects of the dynamic behaviour of a partition wall system. However, a partition wall should not always be analyzed as an isolated homogeneous element. Many other variables influence its behaviour, such as the existence of weak points throughout the element, the acoustic behaviour of the construction elements of the envelope, or the acoustic characteristics of neighboring spaces. Thus, when a partition element separates two closed spaces, the provided sound insulation is not only influenced by the dynamic behaviour of the partition itself but also by the behaviour of each one of the adjacent spaces. Additionally, if the partition element includes an opening or other types of heterogeneity, a coupling effect between spaces can be generated, and the individual dynamic behaviour of each room can be considerably modified. This coupling phenomenon between rooms is well known, but is still a research topic in many fields such as architectural acoustics (see, for example, the recent works by Bradley and Wang, 2009, or by Meissner, 2009).

A number of authors tried to set up more complex models that allow further variables to be taken into account, in an attempt to overcome some of the identified difficulties. Different numerical schemes for predicting the sound insulation of a separating wall between two rooms have been proposed. One such method, the Statistical Energy Analysis (SEA) method, is very suitable for studying problems involving sound transmission, as demonstrated by Craik (1996). However, it is known that the predictions computed using the SEA at lower frequencies are unreliable, and thus the method is not applicable to low-frequency sound transmission. To overcome this difficulty, Steel and Craik (1994) used the SEA together with a Finite Element Method (FEM) model to estimate the sound transmission between walls.

Maluski and Gibbs (2000) used a FEM model to predict the sound insulation between adjacent rooms at low frequency, concluding that the sound insulation is strongly dependent on the modal behavior of the separated compartments.

During the last three decades, the Boundary Element Method (BEM) has become one of the major numerical techniques for solving the problems of wave propagation, particularly in domains involving unbounded or semi-infinite media (see, for example, Godinho and Tadeu, 2002). The major advantage of the BEM over its counterparts, especially the FEM and the Finite Differences Method (FDM), is that it can solve the wave equation when only the boundary interfaces are discretized.

Perhaps the strongest drawbacks of the BEM are its complex mathematical formulation and the fact that it requires prior knowledge of the fundamental solutions, which are available only for some specific types of differential equations with specific boundary conditions. However, for acoustic spaces, with typically homogeneous propagation media, those solutions are well known, and the method has been applied with success, as documented in the reference book by Wu (2000). Another point that should not be neglected is that the accuracy of a BEM model depends on the special treatment of analytical and numerical integration of the singular and hypersingular integrals. This treatment is not trivial in the general case and specific numerical integration strategies need to be devised in some cases to allow for accurately performing those integrations (as is the case of the strategy devised in Telles, 1987). Using a BEM model, Santos and Tadeu (2002) studied the acoustic insulation provided by a single wall with elastic behaviour separating two tunnels. They concluded that the geometry and the dynamic behaviour of the tunnels have a very strong influence on the sound insulation provided by the separating wall. Later, Tadeu and Godinho (2003) used the BEM together with fundamental solutions for an elastic halfspace to analyse the scattering of acoustic waves by movable lightweight elastic screens.

Mostly in the last decade, a different class of numerical methods has been progressively developed. Those methods are usually designated as meshless methods, as they require neither domain nor boundary discretization. Many techniques can be incorporated in this group, such as the MLPG-Meshless-Local-Petrov-Galerkin (Atluri, 2004), Kansa's Method (Kansa, 1990a; 1990b) or the Method of Fundamental Solutions (MFS).The latter technique is, in practice, a boundary-only technique, in which the pressure field within a given domain is reproduced using a linear combination of the effects of virtual sources located outside this domain; in this process, boundary conditions are enforced at a limited number of boundary points, giving rise to a linear system of equations whose unknowns are the amplitudes of the virtual sources. As in the BEM, the MFS also requires a prior knowledge of the fundamental solutions, but its mathematical formulation and computational implementation are considerably simpler, since no numerical integrations are needed; thus, the difficulty of the singular

and hypersingular integrations is avoided. Some recent papers by Fairweather and Karageorghis (1998), by Fairweather *et al.* (2003) and by Golberg and Chen (1999), describe the MFS and some of its possible applications. It is important to note that, despite the simple concept behind the method, many of the published works dealing with the MFS indicate that it can provide very accurate solutions to different types of physical problems, including those related to acoustics and wave propagation, to heat and mass transfer, or to the structural behaviour of solid structures.

Although different studies have been published on the use of this technique in acoustics, they are mostly restricted to solving the Helmholtz equation in problems involving two-dimensional domains. Alves and Valtchev compared the plane waves method and the MFS for acoustic wave scattering (2005). Godinho *et al.* (2006) studied the accuracy of the MFS in the analysis of 2D acoustic and heat transfer problems, concluding that the method is very accurate for the study of smooth geometrical configurations. Later, the same authors (Godinho *et al.*, 2007) implemented the MFS together with domain decomposition techniques to simulate wave propagation around thin elements and cracks.

Interestingly, to the authors' knowledge, the published studies in which the MFS is applied to 3D acoustic problems are very scarce, in particular concerning more complex problems with connected sub-domains. In one of the few published works, António *et al.* (2008) simulated the propagation of sound within a closed space, using a MFS formulation. In that work, the authors used a single-domain formulation and concluded that the accuracy of the method depends on the number and location of the virtual sources.

In the present paper three-dimensional MFS models are implemented to simulate sound propagation between two closed spaces separated by a rigid wall with a heterogeneity. The heterogeneity connecting the two spaces can be either an opening or a panel which allows only partial transmission of the incident energy (see, for example, Mechel, 2002). Since the separating wall is modelled as a thin element, it is necessary to perform domain decomposition to overcome the numerical difficulties associated with thin elements. Two different models are considered here: one of the models performs the full coupling effect between the two spaces, imposing physically consistent continuity conditions; the other treats the two spaces separately, first determining the pressure or normal particle velocity over the interface between sub-domains (just considering the first space), and then imposing those values as boundary conditions when analysing the second sub-domain. Comparison between those models will allow to assess the importance of the coupling effect between the two spaces and its influence on the calculation of the sound pressure level (SPL) reduction.

The present paper is organized as follows: first, the mathematical formulation of the MFS model is presented, together with the fundamental solutions used in its implementation; then, a brief explanation of the domain decomposition technique is given; there follows a verification of the 3D MFS against the reference

analytical solutions known for simple configurations; an experimental validation against laboratorial results obtained for a reduced-scale model is then performed; some applications are presented, illustrating the importance of the coupling effect between rooms when they are connected by an opening; and finally, the coupled MFS model is used to analyze the SPL reduction between two closed spaces connected by an opening or by a lightweight panel.

2. Mathematical formulation

2.1. Sound propagation in 3D spaces

The propagation of sound within a three-dimensional space can be mathematically represented in the frequency domain by the Helmholtz differential equation:

$$\nabla^2 p + k^2 p = 0, \tag{1}$$

where $\nabla^2 = \dfrac{\partial^2}{\partial x^2} + \dfrac{\partial^2}{\partial y^2} + \dfrac{\partial^2}{\partial z^2}$, p is the acoustic pressure, $k = \omega/\alpha$, $\omega = 2\pi f$, f is the frequency and α is the sound propagation velocity within the acoustic medium.

Assuming a point source placed within this propagation domain, at point $\mathbf{x}_0$ with coordinates (x_0, y_0, z_0), it is possible to establish fundamental solutions for the sound pressure G and particle velocity H at a point $\mathbf{x}$ with coordinates (x, y, z), which can be written respectively as

$$G(\mathbf{x}, \mathbf{x}_0, k) = \frac{\mathrm{e}^{-\mathrm{i}kr}}{r}, \tag{2}$$

$$H(\mathbf{x}, \mathbf{x}_0, k, \mathbf{n}) = \frac{1}{-\mathrm{i}\rho\omega} \frac{(-\mathrm{i}kr - 1)\mathrm{e}^{-\mathrm{i}kr}}{r^2} \frac{\partial r}{\partial \mathbf{n}}. \tag{3}$$

In Eqs. (2) and (3), $r = \sqrt{(x - x_0)^2 + (y - y_0)^2 + (z - z_0)^2}$, $\mathbf{n}$ represents the direction along which the particle velocity is to be calculated and ρ is the density of the propagation medium.

2.2. Mathematical formulation of the MFS

The MFS can be used to model the presence of a generic 3D geometry, with different boundary conditions. For this purpose, consider a closed space of arbitrary geometry, as represented in Fig. 1. Assuming that *NS* virtual sources are placed outside the propagation domain, around the closed space, the pressure field can be approximated in terms of a linear combination of fundamental solutions for the governing equation. So, within the propagation domain, the pressure field can be written as

$$p(\mathbf{x}, k) = \sum_{j=1}^{NS} Q_j G(\mathbf{x}, \mathbf{x}_j, k), \tag{4}$$

where $\mathbf{x}_j$ represents the coordinates of the virtual source j (x_j, y_j, z_j), and Q_j is the amplitude of source j. The particle velocity field can be expressed in a similar way.

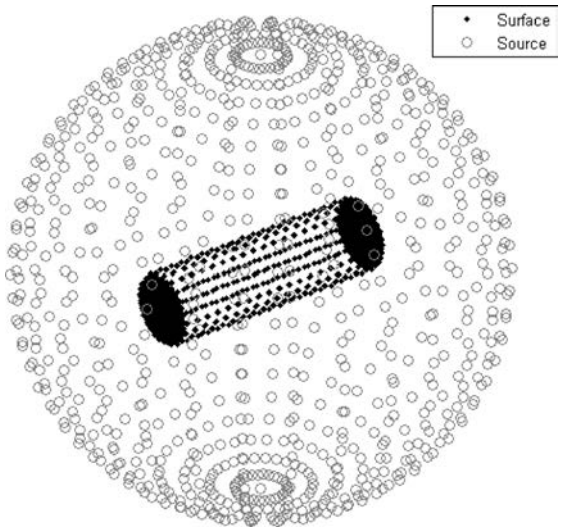

Fig. 1. Generic problem geometry.

If N collocation points are placed over the boundary surface Γ of the closed space, and if the necessary boundary conditions are ascribed at each one of those points, it is possible to establish a system of N equations by NS unknowns. When $N{=}NS$, the system can be solved using standard methods like the Gaussian elimination.

Any boundary condition may be ascribed at each collocation point. The most common boundary conditions will be those of a given particle velocity along the normal direction $(\mathbf{n})$ to the boundary $(v(\mathbf{x}, k, \mathbf{n}) = C)$, a given sound pressure $(p(\mathbf{x}, k) = C)$, or a specific relation between both $(p(\mathbf{x}, k)/v(\mathbf{x}, k, \mathbf{n}) = C)$, which may be used, for example, to simulate an absorbing surface. For the latter, if a totally absorbing boundary for normal incident waves is to be simulated, the corresponding boundary condition will be given by $p(\mathbf{x}, k)/v(\mathbf{x}, k, \mathbf{n}) = \rho\alpha$.

2.3. MFS with multiple domains

The previous formulation can be used in the generic case of a homogeneous domain, without special conditions such as the presence of thin elements or the connection with other domains. However, this formulation can be extended to a more general case making use of multiple domains.

Consider now a system composed of two closed and interconnected domains, Ω_1 and Ω_2, filled with a fluid with density ρ and allowing a sound propagation velocity α.

Considering that $NS1$ sources are distributed around the domain Ω_1, and that $NS2$ sources are placed around the domain Ω_2, the pressure field inside each domain can be written as:

$$p(\mathbf{x},k)_{\Omega_1} = \sum_{j=1}^{NS1} Q_j G(\mathbf{x},\mathbf{x}_{1,j},k) \qquad \text{for } x \text{ in } \Omega_1, \tag{5}$$

$$p(\mathbf{x},k)_{\Omega_2} = \sum_{j=1}^{NS2} P_j G(\mathbf{x},\mathbf{x}_{2,j},k) \qquad \text{for } x \text{ in } \Omega_2, \tag{6}$$

where $k = \omega/\alpha$, Q_j and P_j are the amplitudes of the virtual sources placed around the domains Ω_1 and Ω_2, respectively.

To determine the amplitudes Q_j and P_j, it is necessary to consider a number of collocation points covering the boundary of each domain, where the relevant boundary conditions are imposed. At each collocation point located at the surface connecting the two domains, continuity boundary conditions should be enforced, with $p(\mathbf{x},k)_{\Omega_1} = p(\mathbf{x},k)_{\Omega_2}$ and $v(\mathbf{x},k,\mathbf{n})_{\Omega_1} = v(\mathbf{x},k,\mathbf{n})_{\Omega_2}$. Assuming that the number of collocation points exclusively in Ω_1 is $N1$, that the number of collocation points exclusively in Ω_2 is $N2$, and that the number of common collocation points in the coupling interface is NBC, after imposing the relevant boundary conditions, a set of $N1+N2+2NBC$ equations by $NS1+NS2$ unknowns system may be established, allowing the calculation of the Q_j and P_j unknowns.

To illustrate the construction of the equation system, consider two rooms with rigid walls, connected by an opening. Consider that the $N1$ points are to enforce the null velocity along the boundaries of room 1 ($\overline{\mathbf{x}}_{i,b1}$ being the i-th point) and $N2$ points are used for the same purpose in room 2 ($\overline{\mathbf{x}}_{i,b2}$ being the i-th point); additionally, a number NBC of points ($\overline{\mathbf{x}}_{i,bc}$ being the i-th point) are used to define the opening. Around each room, $NS1$ and $NS2$ virtual sources are used to define the respective sound fields ($\mathbf{x}_{i,j}$ being the i-th source of the room j). For this case, the equation system originated in the presence of a point load located at $\mathbf{x}_{\text{source}}$ within room 1, can be defined as $\mathrm{A}\mathrm{x} = \mathrm{B}$ with:

$$\mathrm{A} = \begin{bmatrix}
H(\overline{\mathbf{x}}_{1,b1},\mathbf{x}_{1,1},k,\mathbf{n}) & \dots & H(\overline{\mathbf{x}}_{1,b1},\mathbf{x}_{NS1,1},k,\mathbf{n}) & 0 & \dots & 0 \\
\vdots & & \vdots & \vdots & & \vdots \\
H(\overline{\mathbf{x}}_{1,b1},\mathbf{x}_{1,1},k,\mathbf{n}) & \dots & H(\overline{\mathbf{x}}_{N1,b1},\mathbf{x}_{NS1,1},k,\mathbf{n}) & 0 & \dots & 0 \\
H(\overline{\mathbf{x}}_{1,bc},\mathbf{x}_{1,1},k,\mathbf{n}) & \dots & H(\overline{\mathbf{x}}_{1,bc},\mathbf{x}_{NS1,1},k,\mathbf{n}) & -H(\overline{\mathbf{x}}_{1,bc},\mathbf{x}_{1,2},k,\mathbf{n}) & \dots & -H(\overline{\mathbf{x}}_{1,bc},\mathbf{x}_{NS2,2},k,\mathbf{n}) \\
\vdots & & \vdots & \vdots & & \vdots \\
H(\overline{\mathbf{x}}_{NBC,bc},\mathbf{x}_{1,1},k,\mathbf{n}) & \dots & H(\overline{\mathbf{x}}_{NBC,bc},\mathbf{x}_{NS1,1},k,\mathbf{n}) & -H(\overline{\mathbf{x}}_{NBC,bc},\mathbf{x}_{1,2},k,\mathbf{n}) & \dots & -H(\overline{\mathbf{x}}_{NBC,bc},\mathbf{x}_{NS2,2},k,\mathbf{n}) \\
G(\overline{\mathbf{x}}_{1,bc},\mathbf{x}_{1,1},k) & \dots & G(\overline{\mathbf{x}}_{1,bc},\mathbf{x}_{NS1,1},k) & -G(\overline{\mathbf{x}}_{1,bc},\mathbf{x}_{1,2},k) & \dots & -G(\overline{\mathbf{x}}_{1,bc},\mathbf{x}_{NS2,2},k) \\
\vdots & & \vdots & \vdots & & \vdots \\
G(\overline{\mathbf{x}}_{NBC,bc},\mathbf{x}_{1,1},k) & \dots & G(\overline{\mathbf{x}}_{NBC,bc},\mathbf{x}_{NS1,1},k) & -G(\overline{\mathbf{x}}_{NBC,bc},\mathbf{x}_{1,2},k) & \dots & -G(\overline{\mathbf{x}}_{NBC,bc},\mathbf{x}_{NS2,2},k) \\
0 & & 0 & H(\overline{\mathbf{x}}_{1,b2},\mathbf{x}_{1,2},k,\mathbf{n}) & \dots & H(\overline{\mathbf{x}}_{1,b2},\mathbf{x}_{NS2,2},k,\mathbf{n}) \\
 & & & \vdots & & \vdots \\
0 & & 0 & H(\overline{\mathbf{x}}_{N2,b2},\mathbf{x}_{1,2},k,\mathbf{n}) & \dots & H(\overline{\mathbf{x}}_{N2,b2},\mathbf{x}_{NS2,2},k,\mathbf{n})
\end{bmatrix}, \tag{7}$$

$$\mathrm{x} = \begin{bmatrix} Q_1 \\ \vdots \\ Q_{NS1} \\ P_1 \\ \vdots \\ P_{NS2} \end{bmatrix} \quad \text{and} \quad \mathrm{B} = \begin{bmatrix} -H(\overline{\mathbf{x}}_{1,b1}, \mathbf{x}_{\text{source}}, k, \mathbf{n}) \\ \vdots \\ -H(\overline{\mathbf{x}}_{N1,b1}, \mathbf{x}_{\text{source}}, k, \mathbf{n}) \\ -H(\overline{\mathbf{x}}_{1,bc}, \mathbf{x}_{\text{source}}, k, \mathbf{n}) \\ \vdots \\ -H(\overline{\mathbf{x}}_{NBC,bc}, \mathbf{x}_{\text{source}}, k, \mathbf{n}) \\ -G(\overline{\mathbf{x}}_{1,bc}, \mathbf{x}_{\text{source}}, k) \\ \vdots \\ -G(\overline{\mathbf{x}}_{NBC,bc}, \mathbf{x}_{source}, k) \\ 0 \\ \vdots \\ 0 \end{bmatrix}. \tag{8}$$

It is important to note that other interface conditions can be simulated at the surface connecting the two spaces. If one assumes that the connection between the two spaces is made by a homogeneous plate of mass m, behaving as a free mass with null damping forces and null stiffness, following the approach described by Mechel (2002), it is possible to establish the following relation between the sound pressure on both sides of the plate and the normal particle velocity at this surface:

$$p(\mathbf{x}, k)_{\Omega_1} - p(\mathbf{x}, k)_{\Omega_2} = \mathrm{i}\omega\, m\, v(\mathbf{x}, k, \mathbf{n})_{\Omega_1}. \tag{9}$$

Additionally, it becomes necessary to enforce continuity of particle velocities between both sides,

$$v(\mathbf{x}, k, \mathbf{n})_{\Omega_1} = v(\mathbf{x}, k, \mathbf{n})_{\Omega_2}. \tag{10}$$

These relations allow the definition of two equations at each collocation point located at the surface connecting the two domains, leading to the necessary $N1 + N2 + 2NBC$ equations by means of the $NS1 + NS2$ unknowns equation system. It is important to note that the presented equation holds its validity only when the incidence of sound waves occurs along the normal to the plate.

As stated in the introduction of this paper, a second approach was also implemented for the analysis of the proposed problems, based on decoupling the two acoustic spaces, and analyzing them separately. For this decoupled approach, when an opening connects the two spaces, the solution sequence can be described as:

- The emitting acoustic space, where an acoustic source is located, is first analysed as a completely independent and closed space, using a single domain MFS model. The MFS model is defined by imposing the relevant boundary conditions at $N1 + NBC$ boundary points and simulating the pressure field using $NS1$ virtual sources (originating a $(N1 + NBC) \times NS1$ system). In this analysis, along the opening's surface (at NBC points) an approximate absorbing condition is imposed, ascribing an impedance of $p(\mathbf{x}, k)/v(\mathbf{x}, k, \mathbf{n}) = \rho\alpha$. At

the remaining boundary points, the adequate conditions are imposed (corresponding either to a rigid or to a partially absorbing surface).

- After solving the previous problem, the normal particle velocities are calculated at the boundary points located along the opening. For this purpose, the particle velocity is determined as $v(\mathbf{x}, k, \mathbf{n})_{\Omega_1} = \sum_{j=1}^{NS1} Q_j H(\mathbf{x}, \mathbf{x}_{1,j}, k, \mathbf{n})$.
- A second model is then built to separately analyze the receiving space. In this model, the calculated values of the particle velocity are imposed as boundary conditions for the second space, at the exact position of the opening. This boundary conditions will act as the source for the second model, originating the pressure field within this space. The problem is then solved for that space using a single domain MFS model. In a similar manner to that used for the first space, the MFS model is here defined by imposing the relevant boundary conditions at $(N2 + NBC)$ boundary points and simulating the pressure field, using $NS2$ virtual sources (originating a $(N2 + NBC) \times NS2$ system).

2.4. Model verification

The work by António *et al.* (2008) revealed that the accuracy of the response computed using a 3D MFS model will significantly depend on the position of the virtual sources, used to simulate the pressure field. For this reason, a preliminary study will be performed, verifying the behaviour of the method against a reference solution known for a simple geometric configuration, with the purpose of defining an adequate position for those sources and to ensure that meaningful results will be obtained. For this purpose, the model is first verified against the analytical solution known for 1D sound propagation near an anechoic surface, and then against a full 3D analytical solution.

Consider a parallelepipedic space, with dimensions of $6 \times 4 \times 2.5$ m, filled with air, with a density of 1.22 kg/m^3 and allowing the sound to propagate at 340 m/s. Assume that all the surfaces of this space are rigid, with null normal particle velocities, except one of the surfaces, at $x = 0$ m, where a boundary condition of $v = 1 \times 10^{-3}$ m/s, along the direction of the inward normal, is ascribed. On the opposite face, an anechoic termination is considered and thus, for this case, the geometry corresponds to a 1D problem in which only plane waves are generated. It then becomes possible to derive the following analytical solution for this problem:

$$p(x, k) = \rho\alpha \mathrm{e}^{-\mathrm{i}kx} \frac{\left(1 + \mathrm{e}^{-2\mathrm{i}k(L-x)}\right)}{\left(1 - \mathrm{e}^{-2\mathrm{i}kL}\right)}, \tag{11}$$

where L is the distance between the vibrating and the anechoic surfaces, and x is the position of the receiver inside the space.

The proposed MFS model has been used to compute the acoustic pressure inside this system, dividing the propagation medium into two separate domains,

and coupling them by imposing full continuity of pressures and normal particle velocities at the interface. For this purpose, 1480 virtual sources were placed around each of the defined subdomains. The boundary points were distributed uniformly along the surfaces of each subdomain, thus leading to a system of 2960 equations by 2960 unknowns. A schematic representation of the boundary points and virtual sources distribution is presented in Fig. 2. It is important to

a)

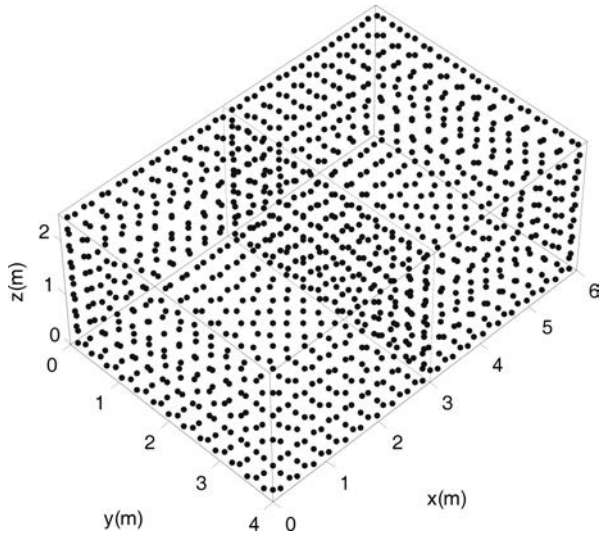

b)

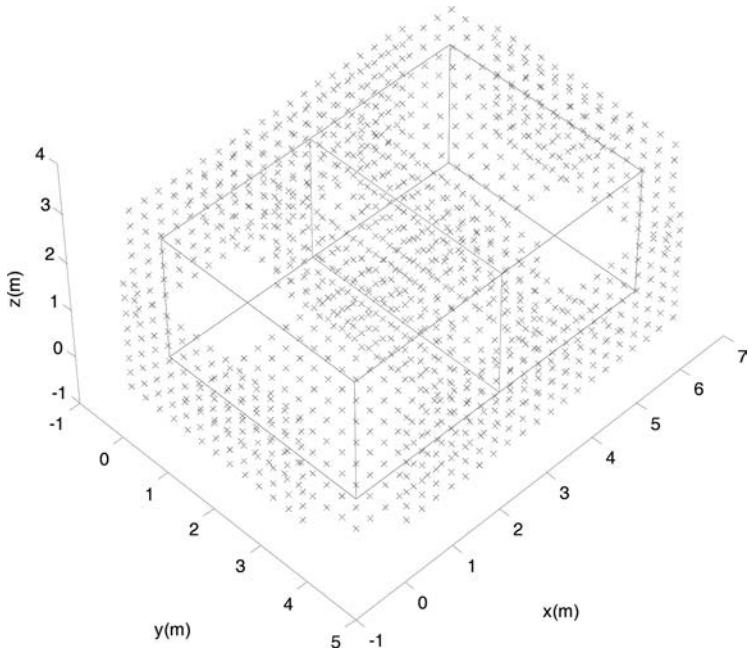

Fig. 2. Schematic representation of the boundary points (a) and virtual sources (b) distribution.

understand that, in this configuration, the intermediate wall, common to the two sub-domains, acts as a coupling interface, along which continuity conditions are enforced.

Figure 3a illustrates the real and imaginary responses computed analytically along the x-axis for a frequency of 250 Hz, while Fig. 3b illustrates the relative error computed for the MFS approximation, calculated as

$$\left| \frac{p_{\text{analytic}} - p_{MFS}}{\max(p_{\text{analytic}})} \right|, \tag{12}$$

a)

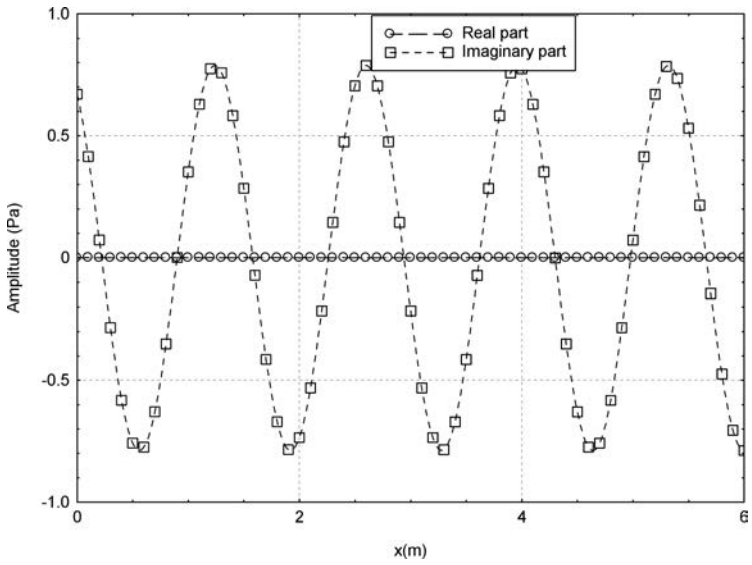

b)

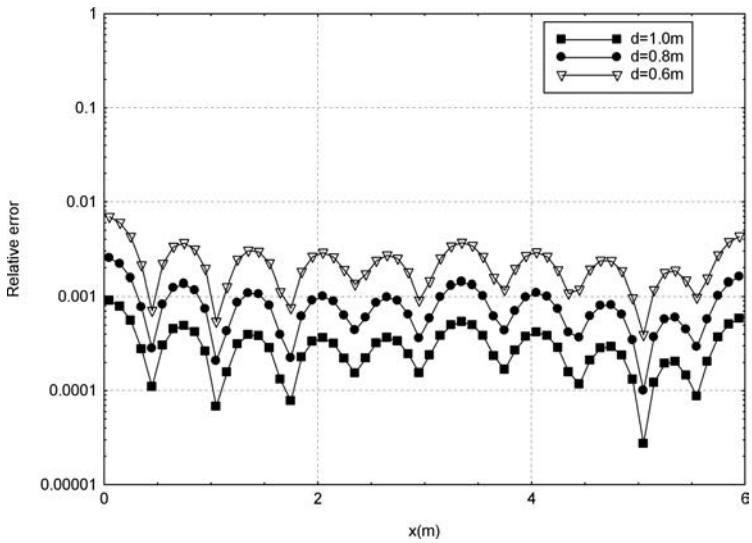

Fig. 3. a) Real and imaginary parts of the analytical solution for a frequency of 250 Hz; b) Relative error computed with the MFS.

when the virtual sources are placed at different positions, at distances 0.6 m, 0.8 m and 1.0 m from the boundary surfaces. It is important to note that the quantities p_{analytic} and p_{MFS} are both complex numbers, and that the modulus is used in Eq. (12) to present the global relative error as a real positive number. Additionally, since the analytical response reaches null values at some domain points, leading to indeterminacy in the result of Eq. (12), the error is normalized with respect to the maximum value of the pressure response within the analyzed points. The figure allows concluding that the MFS solution provides a very good approximation to the analytical solution, thus proving that the implementation of the method is correct. It is also possible to conclude that, for this case, the best results are obtained for virtual sources placed further away from the boundaries of the system. In fact, in this particular case, only plane waves propagate in the system, a field which is best simulated when the point sources are located away from the interior domain so that an almost flat wavefront reaches the receivers.

To better understand the behaviour of the 3D multi-domain MFS model in the presence of a more complex sound field, an additional verification is here performed for the case in which the above described 3D enclosure has a totally rigid envelope, and when the excitation source is a point load with unitary amplitude factor (as given in Eq. (2)) located at ($x = 1.0$ m; $y = 1.0$ m; $z = 1.0$ m). For this case, an analytical solution can be obtained using the image-source method, as described in the literature by Tadeu *et al.* (2000). However, to allow for the definition of such solution using a finite number of virtual sources, a damping factor is introduced in the form of a complex frequency of the type

$$\omega_c = 2\pi f - \mathrm{i} \times 2\xi\pi\Delta f. \tag{13}$$

In this expression, f is the frequency in Hz, Δf is the frequency increment and ξ is the damping factor. For this verification, we use $\xi = 0.7$ and $\Delta f = 4$ Hz. In practice, this damping factor corresponds to attenuating at least 81 times the effect of the virtual sources required for the analytical solution placed further than $1/\Delta f \times 340 = 85$ m. For further details in this respect, the Reader is advised to consult the original work by Tadeu *et al.* (2000). Analytical results (real and imaginary parts) computed at a receiver placed at ($x = 5.0$ m; $y = 2.0$ m; $z = 1.5$ m) are presented in Fig. 4a. In Fig. 4b and 4c, the relative errors computed for the MFS model using Eq. (12) are displayed. The distances between the virtual sources and the boundary are set to 0.6 m, 0.8 m and 1.0 m. As in the previous example, in the MFS model, the enclosure is divided into two sub-domains with equal dimensions, coupled together by a virtual interface located at $x = 3.0$ m. For the results displayed in Fig. 4b, 944 boundary points and virtual sources were used to model each of the sub-domains, while for Fig. 4c, this number was increased to 1480. The results shown in both figures prove that, as in the previous case, the relative errors tend to decrease as the sources are placed further away from the boundary. Additionally, it is clear that, for the higher frequencies, the model benefits from the increase in the number of

a)

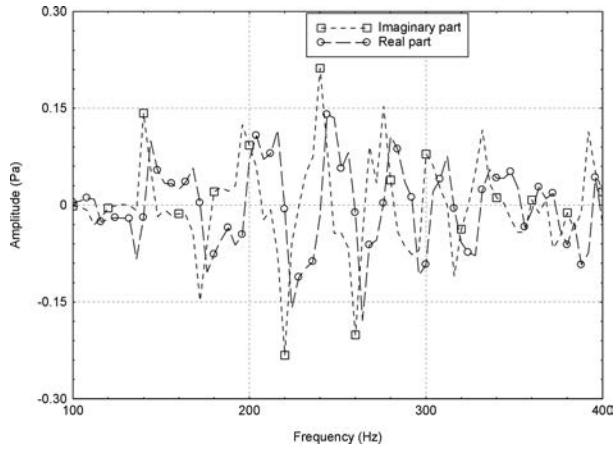

b)

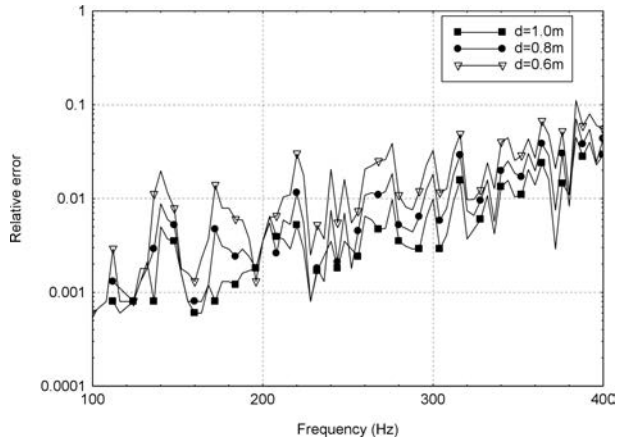

c)

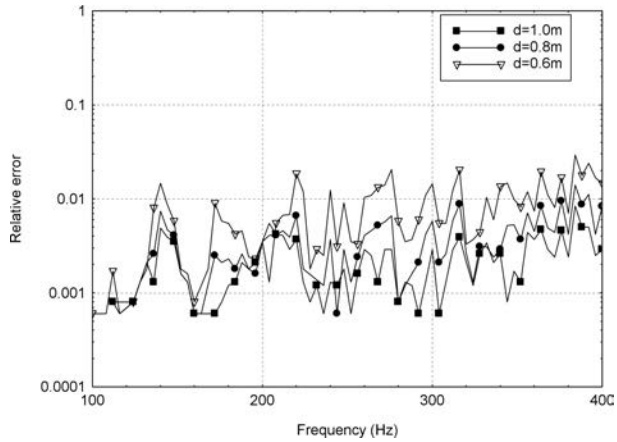

Fig. 4. a) Real and imaginary parts of the analytical solution for a frequency range between 100 Hz and 400 Hz; b) Relative error computed for the MFS using 1888 virtual sources; c) Relative error computed for the MFS using 2960 virtual sources.

boundary points and virtual sources, with the relative error decreasing. For that case, low relative errors are obtained, with values below 1% for all frequencies when the sources are located 1.0 m from the boundary.

3. Experimental validation

To assess the practical applicability of the MFS model in simulation of the sound propagation, it is important first to compare the results it provides with those that can be measured experimentally. For this purpose, a simple experimental setup was developed and subjected to the incidence of sound waves. The model consisted of a reduced-scale parallelepipedic enclosure, with internal dimensions of $0.6 \times 0.4 \times 0.25$ m. These dimensions correspond to scaling down 10 times the geometry defined in the verification examples. The sound waves are introduced in this system through an impedance tube with a diameter of 0.05 m, centered on one of the faces of the enclosure. The use of an impedance tube for this purpose allows to accomplish two main objectives: first, it allows an adequate control of the excitation introduced in the system, ensuring that this excitation can be adequately represented as a plane wave; second, it avoids the use of an acoustic source inside the small-scale model, which would act as a partially absorbing object influencing the pressure field within the acoustic space. On the face opposite to the source, an exit tube was installed, formed by a short PVC tube 0.10 m long, with a diameter of 0.05 m, and with an anechoic termination materialized by a block of rockwool 0.04 m thick, with a density of 70 kg/m^3. The sound pressure level was then measured at the entrance (within the impedance tube) and in the exit tube, at opposite faces of the model, by means of two microphones. Inside the model, an obstacle simulating a rigid wall was introduced, generating a disturbance in the sound field and originating a complex wave pattern within the space. An opening 0.1 m wide was left open, connecting two parts of the experimental model. A schematic representation of this model can be found in Fig. 5a. In this plan view representation, the position of the two microphones, of the plane-wave source and of the internal obstacle, is indicated.

The signal is acquired using a 2-channel "Symphonie" acquisition system, from 01 dB, connected to two GRAS Sound & Vibration 40AF microphones. These are free-field microphones subject to an incidence at an angle of 90°, and thus a corrective term should be introduced at each of them, obtained from the characteristic curve provided by the producer (GRAS Sound & Vibration). However, for this specific microphone model, the correction factor is approximately null up to 3 kHz, and thus it does not influence the measured sound pressure levels within the analyzed frequency range. The response of this system when the impedance tube generates a broad band noise is registered during 6 s, and this test is repeated 5 times. Average SPLs are calculated at each microphone for frequencies up to 1750 Hz. An average SPL reduction is then calculated as the difference between the average SPLs registered at the entrance and exit tubes.

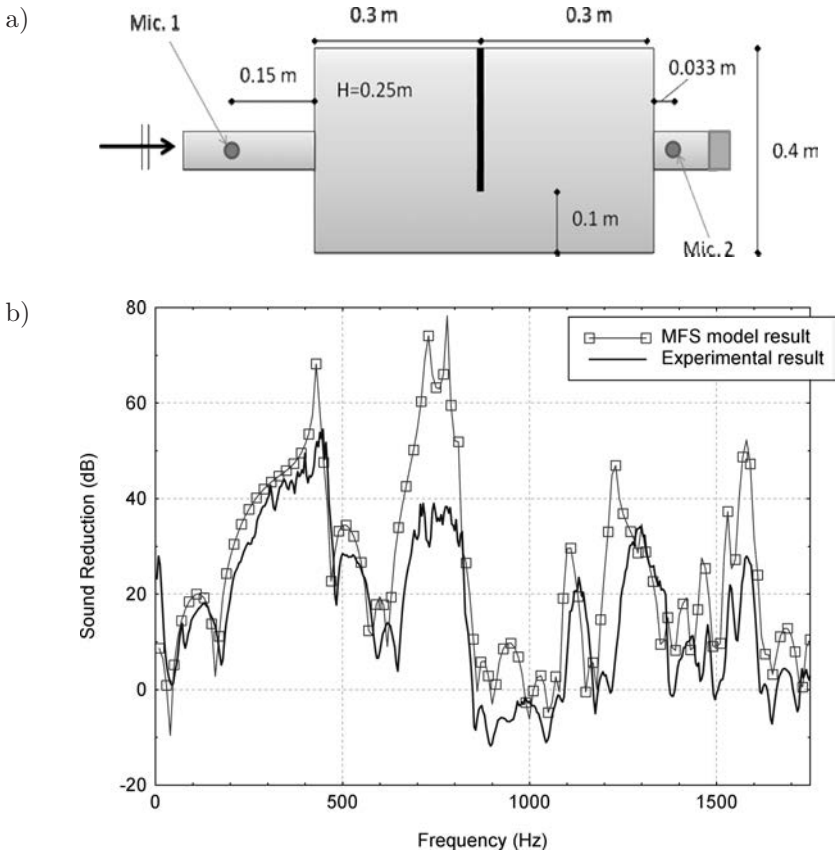

Fig. 5. a) Schematic representation of the validation model (plan view); b) Numerical and experimental curves obtained for the sound reduction in the presence of the given geometry.

Figure 5b illustrates the comparison between experimental and numerical results computed for the defined configuration. Observing this figure, it is possible to conclude that, in general, there is a very good agreement between the measured results and those estimated using the numerical model. In fact, the two curves have very similar trends, with the position of peaks and valleys matching well between both. Some discrepancies occur in what concerns the involved amplitudes, a situation which can be justified by small differences between the experimental apparatus and the modeled geometry. Among these, small misalignment between inlet and outlet and slight variations of the position of the internal obstacle may play an important role.

4. Numerical examples

The proposed numerical formulations were used to study the sound propagation between two rooms. In what follows, two different groups of analyses

will be presented: in a first set, the importance of the coupling effect between the rooms is analysed, making use of a simple configuration in which a rigid barrier partially separates the two spaces; in the second set, the case of two rooms connected by either an opening or a lightweight panel, placed at different positions, is analysed. In all examples, the remaining part of the wall between the two rooms is assumed to be rigid and with thickness tending to zero. Two different wall surface conditions are simulated, namely a completely reflecting surface ($v = 0$ m/s) and a partially absorbing surface. For the latter one, the partially absorbing surface conditions (with an absorption coefficient of $\overline{\alpha} = 0.2$) are ascribed to all the surfaces of both rooms by imposing an impedance with the relation

$$p(\mathbf{x}, k)/v(\mathbf{x}, k, \mathbf{n}) = \rho\, \alpha \frac{1 + \sqrt{1 - \overline{\alpha}}}{1 - \sqrt{1 - \overline{\alpha}}}. \tag{14}$$

One should note that, in this specific case, this equation originates a real impedance value. However, complex impedances may be incorporated in the proposed model using the same approach.

In all the cases presented, both rooms are parallelepipedic with $3 \times 4 \times 2.5$ m, and the sound field within each room is simulated by 1480 virtual sources, placed at a distance of 1.0 m from the boundary. The necessary boundary conditions are enforced by making use of 1480 boundary points covering the whole surface of each room. The propagation media have a density of 1.22 kg/m^3 and allow sound waves to travel at 340 m/s.

4.1. Coupling effect between rooms

The SPL reduction provided by a wall with an opening separating two rooms can be estimated using different methodologies with different degrees of simplification. A common and effective simplification corresponds to decoupling the two spaces and analysing them separately. However, it is important to understand the consequences of such simplification, and to what extent it can affect the accuracy of the results. To assess the importance of that methodology, consider the above described acoustic spaces, separated by a rigid wall up to a height of 1.9 m, and with an opening between the top of this wall and the ceiling. Additionally, consider that the emitting room is excited by a point source positioned at ($x = 1.0$ m; $y = 1.0$ m; $z = 1.0$ m), as illustrated in Fig. 6, oscillating with different frequencies. The response has been computed for 200 frequencies, ranging from 50 Hz to 500 Hz, calculating the response at two distinct sets of receivers, placed within each of the rooms. These receivers are positioned in a regular 3D grid of 240 receivers, equally spaced of 0.5 m along each direction. The average sound pressure level inside each room (L1 and L2) has been computed using these two grids, and the SPL reduction between them has been calculated as L1-L2.

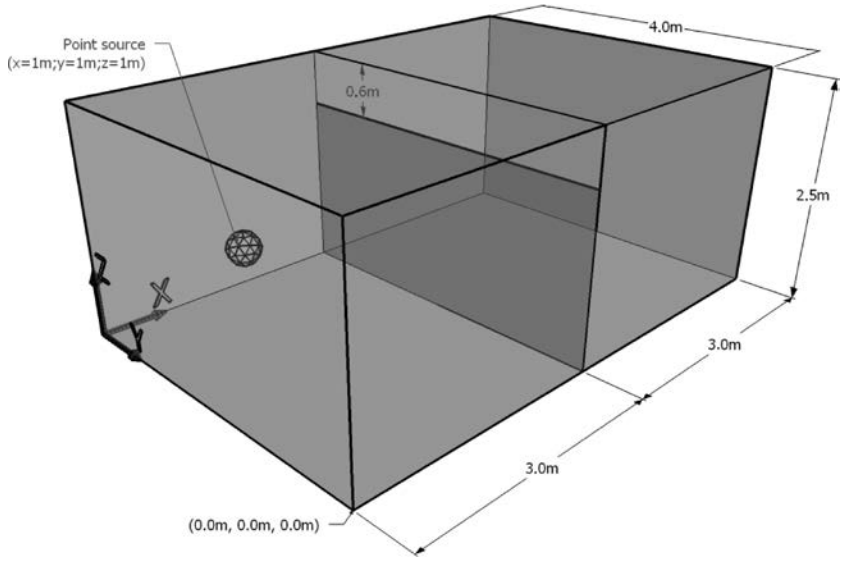

Fig. 6. Schematic representation of the problem.

Figure 7a illustrates the SPL reduction curve computed using both a fully coupled model and a decoupled model, when the surfaces of the walls are completely rigid. For both models, the computed SPL reduction curve shows pronounced variations along the frequency domain, exhibiting a strong oscillatory behaviour with a sequence of dips. Analyzing the position of these dips in the frequency domain, it becomes possible to relate them to stationary wavefields generated inside both rooms. For parallelepipedic rooms, in the absence of any opening, it is possible to compute analytically these eigenfrequencies as:

$$f_{n,m,p} = \frac{\alpha}{2}\sqrt{\left(\frac{n}{L_x}\right)^2 + \left(\frac{m}{L_y}\right)^2 + \left(\frac{p}{L_z}\right)^2} \tag{15}$$

where n, m and p are the order numbers of the mode along the directions x, y and z, and L_x, L_y and L_z are the dimensions of the room along those directions. For the analysed system, this equation allows to conclude that the first modes of the rooms occur at $f_{1,0,0} = 56.7$ Hz, $f_{0,1,0} = 42.5$ Hz, $f_{0,0,1} = 68.0$ Hz, $f_{1,1,0} = 70.8$ Hz, $f_{1,0,1} = 88.5$ Hz, $f_{0,1,1} = 80.2$ Hz and $f_{1,1,1} = 98.2$ Hz.

To allow a more accurate comparison, the position of these modes is also represented in Fig. 7b together with a zoomed view of the SPL reduction curves. Interestingly, the SPL reduction dips are slightly shifted from the calculated frequencies when the coupled model is used, but they match almost exactly when a decoupled analysis is performed. In fact, in presence of the opening, the coupling between the two rooms introduces a variation in the dynamic behaviour of the system, changing the positions of the acoustic modes of each individual room. For example, in the case of the first acoustic mode, in presence of the opening it

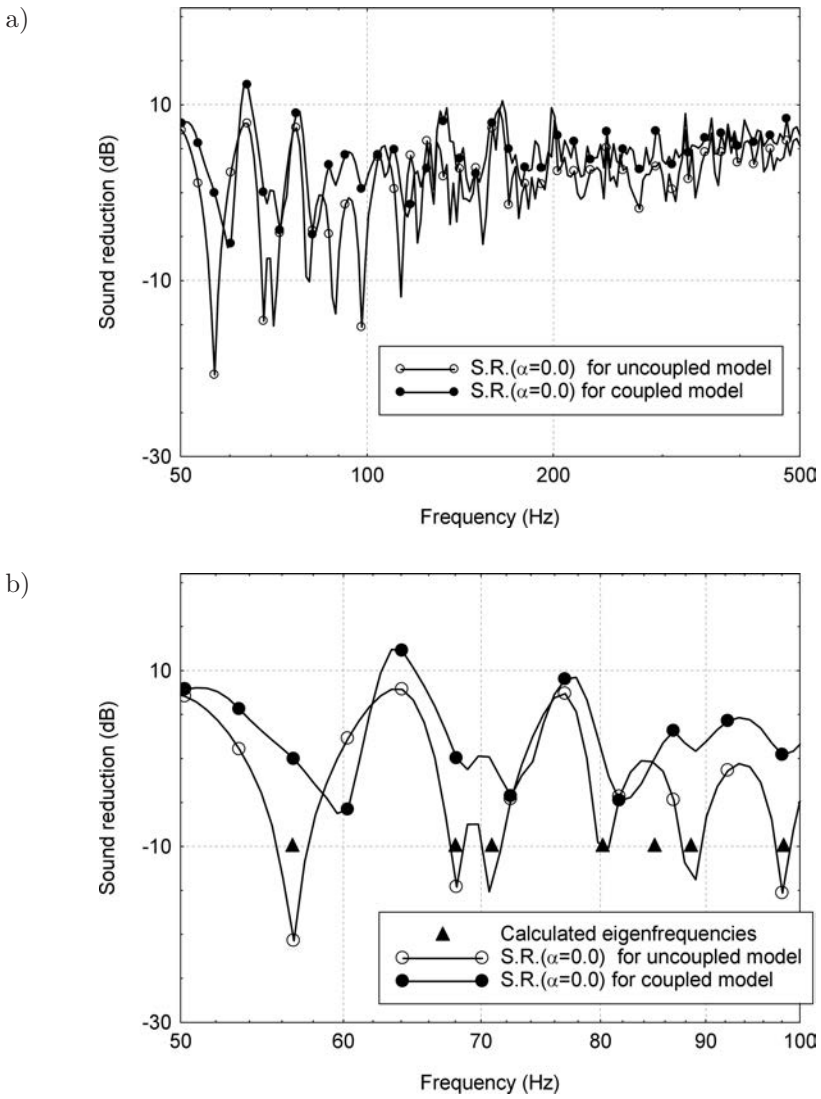

Fig. 7. Sound pressure level reduction curves for the two models considering perfectly reflective walls: a) analyzed frequency range; b) zoomed view between 50 Hz and 100 Hz.

occurs around 61 Hz, being shifted by approximately 4 Hz above the frequency estimated by Eq. (15). By contrast, if a decoupled analysis is performed, the dynamic behaviour of each individual room is maintained, and thus the frequency position of the SPL reduction dips coincides with the predicted values.

It is interesting to note that, globally, the trends of the curves predicted by the two models are quite similar, particularly at the upper frequencies of the analyzed frequency range. In fact, the decreasing influence of diffraction for higher frequencies helps to explain the reduction in dips and peaks registered

for the model with non-absorbing surfaces. However, in considering the low-frequency SPL reduction values, the differences between the two approaches are very significant, and indicates the importance of considering the full coupling between spaces. A similar analysis was performed in the case of an absorbing room (with homogeneous internal surfaces with $\overline{\alpha} = 0.2$), and the corresponding results are presented in Fig. 8. Once again, both the coupled and the uncoupled models present predictions of the same order of magnitude (around 10 dB for the higher frequencies, and lower below 100 Hz), but with visible differences between the two curves. Those differences are more pronounced at lower frequencies, where the first normal modes of the acoustic spaces are located, while for the upper frequency range the two curves are very close to each other.

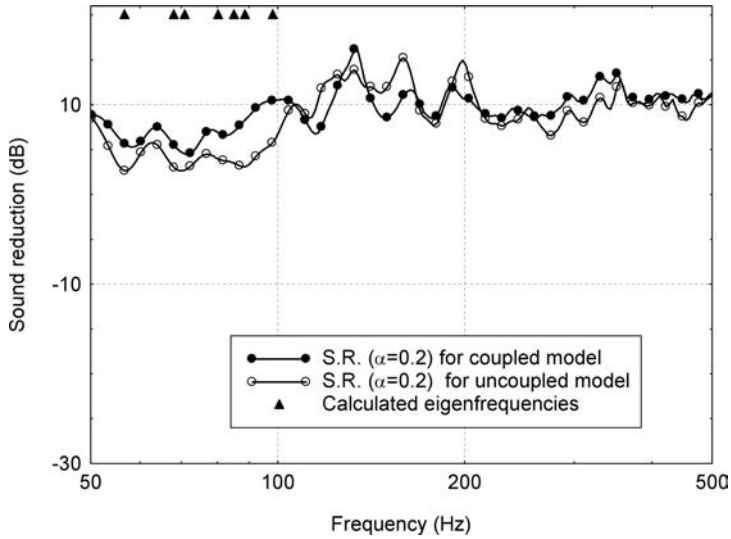

Fig. 8. Sound pressure level reduction curves for the two models considering all internal surfaces with an absorption coefficient of 0.2.

Besides the coupling effect, it is interesting to analyse the behaviour of the system in what concerns the efficiency of the barrier. For this purpose, in Fig. 9 the 1/3 octave band SPL reduction curves calculated using the coupled model are presented for the cases of rigid and absorbing walls. The difference between the magnitudes of the SPL reduction is very clear, and indicates the advantage of considering an absorbing treatment for the walls, ceiling and floor. For that case, the multiple reflections occurring within each space are greatly attenuated, since part of the sound energy is dissipated when the sound waves reach various surfaces. For the case of rigid walls, the effect of the barriers at the lower frequency bands can be considered to be null, with the lower order acoustic modes of the rooms dominating the response. For higher frequencies, this reduction steadily increases and reaches 7 dB for the 400 Hz 1/3 octave band. If the walls

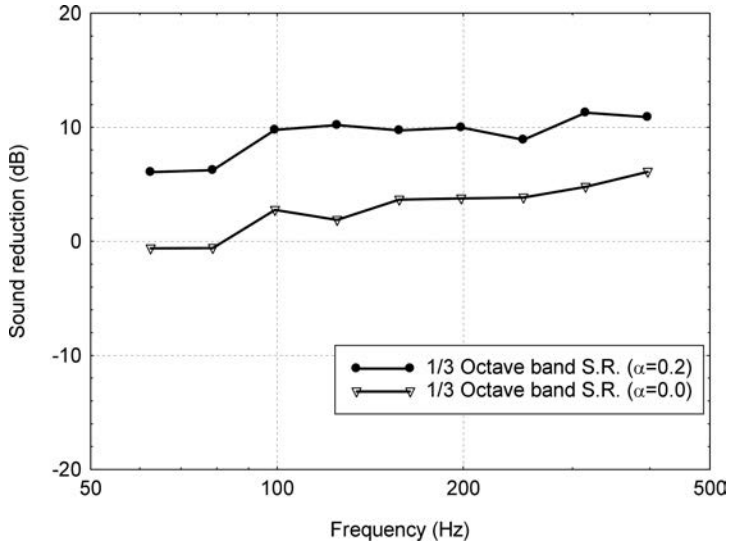

Fig. 9. 1/3 Octave band sound pressure level reduction curves for the case of a barrier between the two rooms.

are modelled as absorbing surfaces, even at lower frequencies a SPL reduction of around 7 dB is achieved, and these values become significantly higher above 100 Hz, reaching a maximum of around 11 dB.

4.2. SPL reduction in the presence of a smaller heterogeneity

Let us consider, in this section, the case in which the wall separating the two rooms includes a smaller heterogeneity, which can either be an opening or a lightweight panel. For all cases analyzed here, consider that this heterogeneity is square, with dimensions of 1×1 m. Two different positions of the heterogeneity are considered, what can be seen in Fig. 10a.

For the first set of analysis, consider the heterogeneity to be an opening, along which the continuity conditions are imposed.

When the surfaces of the walls are completely rigid, the computed SPL reduction curve exhibits, as before, pronounced variations along the frequency domain, with a strong oscillatory behaviour and a sequence of dips (see Fig. 10b). Analyzing the position of these dips in the frequency domain, it becomes possible to relate them with stationary wavefields generated inside both rooms, but these SPL reduction dips are slightly shifted from the calculated natural frequencies of the acoustic spaces. This phenomenon was observed in the previous section and it is due to the existence of an opening which modifies the dynamic behaviour of the rooms by making them behave as two coupled domains. In spite of the coupling area being considerably smaller than in the previous cases, this effect can still be easily seen in the presented results.

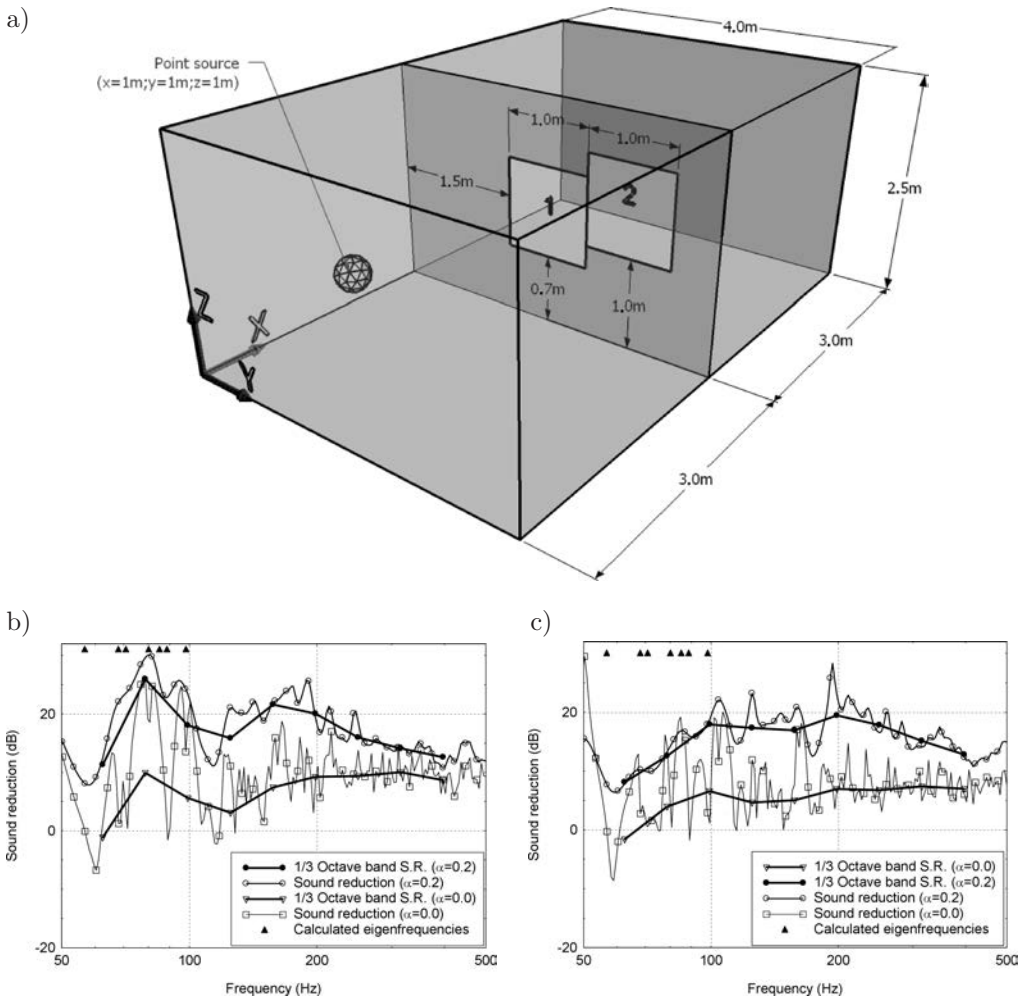

Fig. 10. Two rooms connected by a wall with a 1×1 m opening: a) system geometry; b) sound pressure level reduction when the opening is at position 1; c) sound pressure level reduction when the opening is at position 2.

A SPL reduction curve is also plotted in Fig. 10b, computed for the case in which all surfaces have an absorbing treatment (with $\overline{\alpha} = 0.2$). Since these boundary conditions strongly contribute to attenuate the stationary wavefields, by absorbing a part of the energy, the SPL reduction curve is now smoother, revealing less pronounced dips at the natural frequencies of the rooms. Additionally, due to this absorbing effect, the sound reduction appears to be consistently higher in this situation.

The SPL reduction curves were also calculated for 1/3 octave bands and are shown in the same figure. For comparison purposes, a simplified approach has been used for calculating the SPL reduction provided by this configuration, in

which the sound transmission coefficient is assumed to be $\tau = 1$ in the opening and 0 over the rest of the rigid wall. Using this approach, the reduction can be estimated by weighting the areas of the opening and of the wall, and applying the equation

$$R = 10 \log \left(\left(\frac{A_{\text{opening}} \tau_{\text{opening}} + A_{\text{wall}} \tau_{\text{wall}}}{A_{\text{opening}} + A_{\text{wall}}} \right)^{-1} \right), \tag{16}$$

where A_{wall} and A_{opening} are, respectively, the areas of the wall and of the opening. For the tested configuration, a SPL reduction of 10 dB is predicted by this equation.

Comparing the computed curves for 1/3 octave bands with the prediction by the simplified method, it can be seen that there are significant differences between them. In fact, the SPL reduction predicted by Eq. (16) is significantly different from that predicted by the proposed model with reflecting surfaces, since it neglects the modal behaviour of the two rooms. The reduction predicted by the MFS strongly varies with the frequency, but it seems to be, on average, below the 10 dB value predicted by Eq. (16). However, it is interesting to note that when the absorbing walls are modelled, the SPL reduction increases above this value, and that it seems to approach 10 dB as the frequency increases.

In a second simulation, the opening is considered to be at position 2. Observing the SPL reduction curve (see Fig. 10c) along the frequency domain, it becomes possible to conclude that most of the oscillatory behaviour of the SPL reduction curve is still present, although with a tendency for the SPL reduction to be lower than in the previous case. Analyzing the 1/3 octave band curves, it becomes evident that, globally, they have the behaviours slightly different from the previous case, mainly around 70–80 Hz, in which the SPL reduction decreases in this second situation. Once again, for the case of absorbing walls, the dips in the SPL reduction curve are attenuated, originating a sensible increase in sound reduction.

Consider now a second case consisting of a rigid wall (with null sound-transmission coefficient) within which a small lightweight panel is located. For this case, simplified interface conditions are ascribed to the plate, following those indicated in Eqs. (9) and (10). To allow application of those equations, this plate is assumed to behave as a rigid body and its resonances are not taken into account. In this system, a 1×1 m plate, with a mass of 25 kg/m^2, is embedded within the wall that separates the two rooms. Two different situations are modelled, corresponding to perfectly rigid or absorbing ($\overline{\alpha} = 0.2$) interior surfaces.

Figure 11 illustrates the results computed when the sound field is generated by the same point load used in the previous examples, and when the lightweight panel is located either in position 1 (Fig. 11a) or 2 (Fig. 11b). In these figures, the SPL reduction predicted by the proposed MFS model is plotted together with the reduction predicted by a simplified calculation based on the mass law

a)

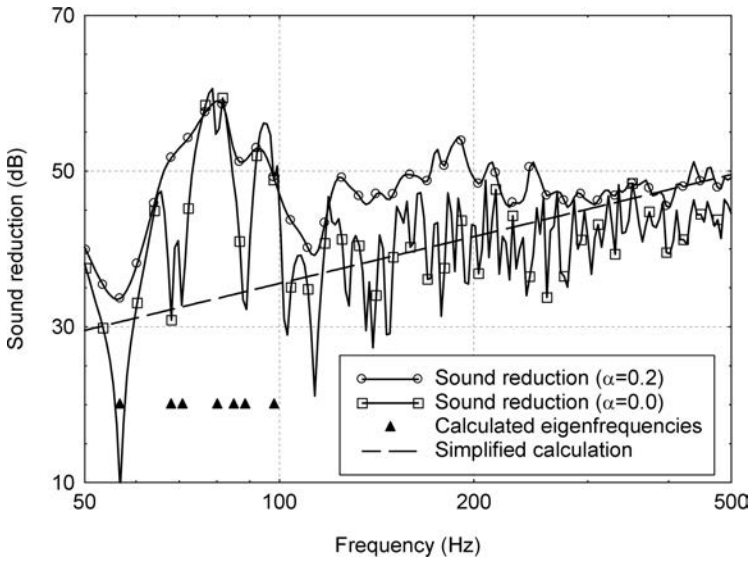

b)

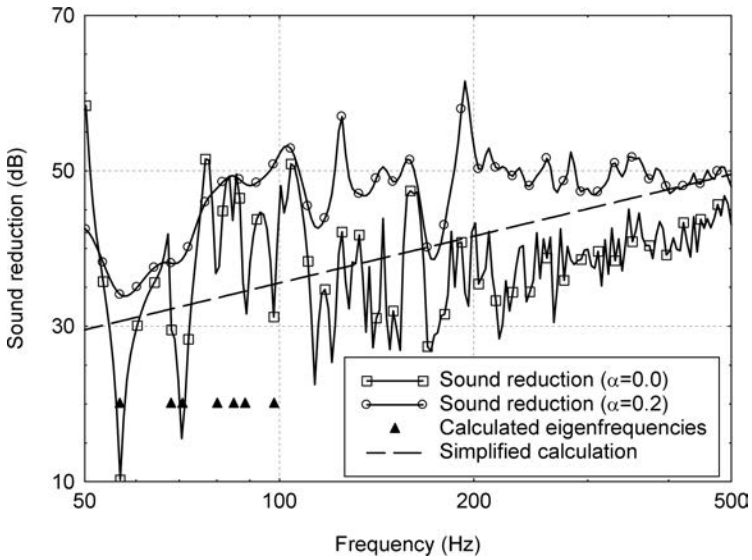

Fig. 11. Sound pressure level reduction when the two rooms are connected by a wall with a 1×1 m lightweight panel: a) results for lightweight plate in position 1; b) results for lightweight plate in position 2.

and in Eq. (16). This simplified approach predicts that the SPL reduction provided by the separation element increases with the frequency, with a slope of 6 dB/octave. It is interesting to note that the computed curves seem to approach the simplified calculation tendency for the higher frequencies, with the SPL reduction increasing when the frequency also increases.

Analyzing the plots in Figure 11a, the SPL reduction curve predicted by the MFS model when the walls are rigid, reveals a strong oscillatory behaviour, with very few similarities to the SPL reduction curve of the simplified model in the lower frequency range. Due to the presence of a point source and to the influence of the acoustic modes of the room, a diffused field is generated within the emitting room, and thus originates a much more complex behaviour than that predicted by the simplified approach. The strong oscillations observed in the SPL reduction curve can be explained by the influence of these acoustic modes excited inside each room, with multiple reflections occurring at various surfaces of each room. It is worth noting that additional oscillations and insulation dips would be visible if the plate was modelled as an elastic solid structure, due to the contribution of its structural resonances. It is interesting to note that, comparing with the case of the opening analyzed above, there seems to be a better correspondence between the calculated eigenfrequencies and the SPL reduction dips. This may be explained by the fact that the presence of the plate leads to a weaker coupling between the two spaces, whose dynamic behaviour is now much more similar to that of isolated (non-connecting) rooms. When the internal surfaces of the rooms are absorbing, the identified effects are greatly attenuated, originating a much smoother curve. For that case, the predicted SPL reduction is consistently above the simplified prediction, particularly at low frequencies, but tends to approach its values for the upper frequencies of the analysis interval.

When the plate is in position 2 (Fig. 11b) and the internal surfaces are perfectly reflective, some changes are observable in the SPL reduction curve, although it still maintains its oscillatory behaviour. Once again, the position of the eigenfrequencies is very close to the theoretical predictions, since the two rooms now have dynamic behaviours close to those of uncoupled spaces. The curve computed for the case of absorbing walls reveals a behaviour similar to the one described in Figure 11a, although the amplitudes of the observed peaks and dips exhibit some variations.

For a final comparison, Fig. 12 illustrates the 1/3 octave SPL reduction curves computed for the 8 configurations analyzed in this section, including the two positions of the opening and of the panel, and both the absorbing and non-absorbing boundary conditions. Clearly, these curves can be identified in groups of two, each pair corresponding to the calculation obtained for the two positions of the opening or panel in a specific scenario. Here, it becomes possible to confirm that the influence of the position of the interface that couples the two spaces has only a significant influence at low frequencies, in which the low-order normal modes of the room have a strong contribution. When the frequency increases, the differences are greatly reduced and, for all pairs, the two curves have similar behaviours. Additionally, it is clear that the effect of an absorbing surface is very significant, originating large differences in the low frequency range, which can reach almost 20 dB. At higher frequencies, this difference is smaller and can be as small as 5 dB. Finally, the curves that correspond to a connection

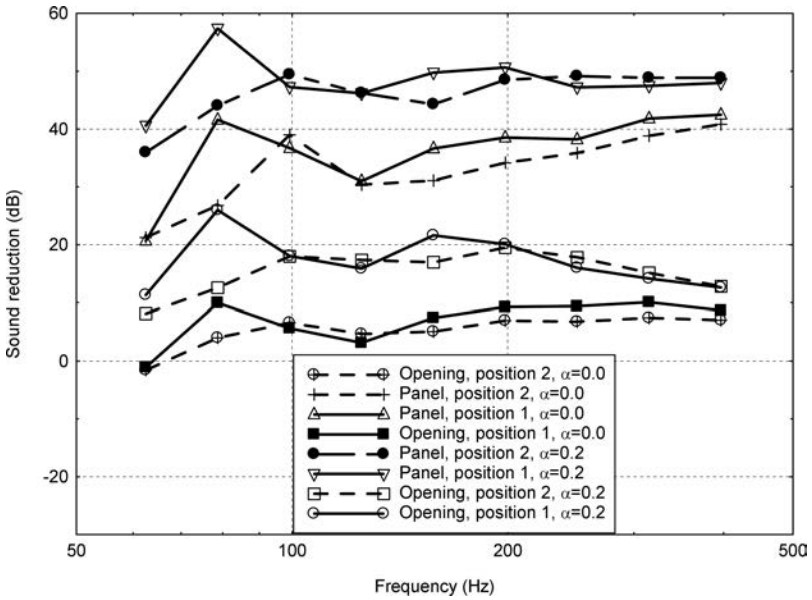

Fig. 12. 1/3 Octave band sound pressure level reduction curves for the studied cases.

between rooms via a lightweight panel, exhibit distinctly higher SPL reductions, a behaviour that was expected and which confirms the strong effect of an opening in reducing the performance of a separating wall.

5. Conclusions

In this paper, a numerical model based on the MFS is proposed to simulate the sound propagation between two rooms with a small connecting area. Both a fully coupled multi-domain model and a decoupled model were implemented and tested. Two different connection types were modelled, namely an opening, allowing all the incident energy to travel without attenuation, and a lightweight panel of a known mass, with a behaviour similar to that predicted by the mass law. The proposed model has been tested against analytical solutions, revealing a good accuracy. An experimental validation was also performed, indicating that the results predicted by the model are close to those found in laboratory tests. It is important to observe here that the presented technique may easily be generalized to problems involving a larger number of sub-domains.

The MFS approach was used to simulate several test cases. The results obtained when the connection between the rooms is an opening, exhibit a behaviour which is consistent with the expected physical behaviour of the systems. The eigenfrequencies of the coupled rooms were identified and associated with pronounced dips in the SPL reduction curve. In the case of an opening connecting the two rooms, the coupling effect between the two acoustic spaces was found

to be significant, with a shift in the eigenfrequencies being clearly identifiable in the response.

When the presence of a lightweight panel is simulated, the calculated results exhibit important differences as compared with those predicted by a simplified model based on the mass law, mainly at lower frequencies. Although the behaviour of the plate is also simulated similarly to the mass law, the complex wavefield generated within each of the rooms markedly influences the SPL reduction between the rooms. For this case, the coupling between the two spaces was found to be weaker and the eigenfrequencies of the coupled systems were very close to those found for the individual spaces.

References

1. Alves C., Valtchev S. (2005), *Numerical comparison of two meshfree methods for acoustic wave scattering*, Engineering Analysis with Boundary Elements, **29**, 371–82.
2. António J., Tadeu A., Godinho L. (2008), *A three-dimensional acoustics model using the method of fundamental solutions*, Engineering Analysis with Boundary Elements, **32**, 525–531.
3. Atluri S.N. (2004), *The Meshless Method (MLPG) for Domain and BIE Discretizations*, Tech. Science Press, USA.
4. Beranek L. L., Vér I.L. (1992), *Noise and Vibration Control Engineering, Principles and Applications*, Wiley, New York, USA.
5. Bradley D., Wang L. (2009), *Quantifying the Double Slope Effect in Coupled Volume Room Systems*, Journal of Building Acoustics, **16**, 2.
6. Craik R. (1996), *Sound Transmission Through Buildings Using Statistical Energy Analysis*, Gower Publishing Limited, Hampshire, England.
7. Fairweather G., Karageorghis A. (1998), *The method of fundamental solutions for elliptic boundary value problems*, Adv. Comput. Math., **9**, 69–95.
8. Fairweather G., Karageorghis A., Martin P.A. (2003), *The method of fundamental solutions for scattering and radiation problems*, Engineering Analysis with Boundary Elements, **27**, 759–69.
9. Godinho L., Tadeu A. (2002), *The Importance of a Small Wall Deformation in the Three-Dimensional Acoustic Logging Results*, Geophysical Journal International, **151**, 2, 403–415.
10. Godinho L., Tadeu A., Amado–Mendes P. (2007), *Wave propagation around thin structures using the MFS*, Computers Materials & Continua (CMC), **5**, 2, 117–127.
11. Godinho L., Tadeu A., Simões N. (2006), *Accuracy of the MFS and BEM on the analysis of acoustic wave propagation and heat conduction problems*, [in:] Advances in the Meshless Method: 2005, J. Sladek, V. Sladek and S.N. Atluri [Eds.], Techscience Press, USA.
12. Golberg M., Chen C.S. (1999), *The method of fundamental solutions for potential, Helmholtz and diffusion problems*. Boundary Integral Methods: Numerical and Mathematical Aspects, Computational Engineering, Vol. 1. Boston, MA: WIT Press/Computational Mechanics Publications, p. 103–176.

13. Kansa E. (1990a), *Multiquadrics – A scattered data approximation scheme with applications to computational fluid-dynamics – I: Surface approximations and partial derivative estimates*, Comput. Math. Appl., **19**, 127–145.

14. Kansa E. (1990b), *Multiquadrics – A scattered data approximation scheme with applications to computational fluid-dynamics – II: Solutions to parabolic, hyperbolic and elliptic partial differential equations*, Comput. Math. Appl., **19**, 147–161.

15. Maluski S., Gibbs B. (2000), *Application of a finite-element model to low-frequency sound insulation in dwellings*, Journal of the Acoustical Society of America, **108**, 4, 1741–1751.

16. Marburg S., Nolte B. (2008), *Computational Acoustics of Noise Propagation in Fluids: Finite and Boundary Element Methods*, Springer-Verlag, Berlin, Germany.

17. Mechel F. (2002), *Formulas of Acoustics*, SpringerVerlag, Berlin, Germany.

18. Meissner M. (2009), *Computer modelling of coupled spaces: variations of eigenmodes frequency due to a change in coupling*, Archives of Acoustics, **34**, 2, 157–168.

19. Santos P., Tadeu A. (2002), *Acoustic insulation provided by a single wall separating two contiguous tunnels via BEM*, Journal of Sound and Vibration, **257**, 5, 945–965.

20. Sharp B.H. (1978), *Prediction methods for the sound transmission of building elements*, Noise Control Engineering Journal, **11**, 53–63.

21. Steel J., Craik R. (1994), *Statistical energy analysis of structure-borne sound transmission by Finite Element Methods*, Journal of Sound and Vibration, **178**, 553–561.

22. Tadeu A., António J. (2002), *Acoustic insulation of single panel walls provided by analytical expressions versus the mass law*, Journal of Sound and Vibration, **257**, 3, 457–475.

23. Tadeu A., António J., Godinho L. (2000), *Frequency and Time Numerical Solutions of 3D Sound Propagation in Open and Closed Spaces*, Journal of Building Acoustics, **7**, 4, 247–261.

24. Tadeu A., Godinho L. (2003), *Scattering of acoustic waves by movable lightweight elastic screens*, Engineering Analysis with Boundary Elements, **27**, 3, 215–226.

25. Telles J. (1987), *A self-adaptive co-ordinate transformation for efficient numerical evaluation of general boundary element integrals*, International Journal for Numerical Methods in Engineering, **24**, 5, 959–973.

26. Wu T. [Ed.] (2000), *Boundary element acoustics*, WIT Press, Southampton, UK.